Near Surface 2009

B11

Rapid Parallel Computation of Optimised Arrays for Electrical Imaging Surveys

M.H. Loke* (Geotomo Software) & P. Wilkinson (British Geological Survey)

SUMMARY

Modern automatic multi-electrode survey instruments have made it possible to use non-traditional arrays to maximise the subsurface resolution from electrical imaging surveys. One of the best methods for generating optimised arrays is to select the array configurations that maximises the model resolution for a homogeneous earth model. The Sherman-Morrison Rank-1 update is used to calculate the change in the model resolution when a new array is added to a selected set of array configurations. This method had the disadvantage that it required several hours of computer time. The algorithm was modified to calculate the change in the model resolution rather than the entire resolution matrix. This reduces the computer time and memory required and also the round-off errors. The matrix-vector multiplications for a single add-on array were replaced with parallel matrix-matrix multiplications for 512 add-on arrays using the computer GPU for the calculations. These changes reduced the computer time by more than two orders of magnitude. The damped and smoothness-constrained least-squares formulations were used in the array optimisation model resolution equation. The smoothness-constrained method can improve the model resolution for deep extended structures where the resolution is poor.

Introduction

In the past decade there have been many significant developments in the resistivity exploration method such that it is now one of the standard techniques used in engineering, environmental and mining surveys. Two-dimensional resistivity surveys, and even three-dimensional surveys, are now widely carried out (Auken et al., 2006, Bingham et al., 2006). The development of automatic multi-electrode survey instruments has made such surveys fast and economical. It has also enabled the user to select the optimum array for the survey problem. Most surveys still use the traditional arrays such as the Wenner, Schlumberger and dipole-dipole. Recently there have been significant developments in algorithms to automatically select arrays to maximise the resolution of the subsurface inversion model (Stummer et al., 2004). A non-linear method that directly calculates the model resolution (the 'Compare R' method) by Wilkinson et al. (2006) proved to be the best method (Loke et al., 2007). However, the 'Compare R' method had the disadvantage of requiring much more computer time. In this paper, the numerical and computational techniques devised to reduce the computer time are described, followed by tests of the arrays using a synthetic model.

Theory

The smoothness-constrained least-squares optimisation method is frequently used for 2-D inversion of resistivity data (Loke et al., 2003). The subsurface model usually consists of a large number of rectangular cells. The linearised least-squares equation that gives the relationship between the model parameters and the measured data is given below.

$$\left(\mathbf{G}^{\mathrm{T}}\mathbf{G}+\lambda\mathbf{C}\right)\Delta\mathbf{r}_{\mathbf{i}}=\mathbf{G}^{\mathrm{T}}\mathbf{g}-\lambda\mathbf{C}\,\mathbf{r}_{\mathbf{i-1}}\,, \tag{1}$$

The Jacobian matrix **G** contains the sensitivities of the measurements with respect to the model parameters, **C** contains the roughness filter constraint, λ is the damping factor and **g** is the data misfit vector. $\mathbf{r_{i-1}}$ is the model parameter vector (the logarithm of the model resistivity values) for the previous iteration, while $\Delta\mathbf{r_i}$ is change in the model parameters. The model resolution matrix **R** (Wilkinson et al., 2004) is given by

$$\mathbf{R}=\left(\mathbf{G}^{\mathrm{T}}\mathbf{G}+\lambda\mathbf{C}\right)^{-1}\mathbf{G}^{\mathrm{T}}\mathbf{G}\ . \tag{2}$$

The main diagonal elements of **R** that give an estimate of the model cells resolutions have values of between 1.0 (for perfect resolution) and 0.0 (no resolution). The 'Compare R' method by Wilkinson et al. (2004) attempts to determine the set of array configurations that will maximise the average resolution value for a homogeneous earth model.

For a system with N electrodes, there are $N(N\text{-}1)(N\text{-}2)(N\text{-}3)/8$ independent four-electrode configurations. To reduce the number of possible arrays, arrays with the Wenner-γ type configuration as well as those large geometric factors are excluded (Stummer et al. 2004). A local optimisation procedure is used to select a subset of the viable configurations (the comprehensive data set) that will maximise the model resolution (Wilkinson et al., 2006). A small base data set consisting of the dipole-dipole configurations with an '*a*' spacing of 1 unit and '*n*' values of 1 to 6 is initially selected. The change in the model resolution matrix **R** for each new array when added to the base set is then calculated. A specified number of configurations that give the largest increase in the model resolution are then added to the base set. This is repeated until the desired number of optimised array configurations is selected. For the following discussion, we rewrite equation (2) into the following form.

$$\mathbf{R}\ =\mathbf{B}\ \mathbf{A}\ \ \text{, where}\quad \mathbf{A}=\mathbf{G}^{\mathrm{T}}\mathbf{G}\ \text{ and }\ \mathbf{B}=\left(\mathbf{G}^{\mathrm{T}}\mathbf{G}+\lambda\mathbf{C}\right)^{-1} \tag{3}$$

The Sherman-Morrison Rank-1 update used to calculate the new resolution matrix $\mathbf{R_{b+1}}$ when a new array is added to the base set is given below.

$$\mathbf{A}_{\mathbf{b+1}}=\mathbf{A}_{\mathbf{b}}+\mathbf{g}\otimes\mathbf{g}\,,\quad \mathbf{B}_{\mathbf{b+1}}=\mathbf{B}_{\mathbf{b}}-\frac{\mathbf{z}\otimes\mathbf{z}}{1+\mu}\,,\qquad \mathbf{R}_{\mathbf{b+1}}=\mathbf{B}_{\mathbf{b+1}}\mathbf{A}_{\mathbf{b+1}} \tag{4}$$

g is the Jacobian vector for the new array, **z**=**Bg**, μ = **g.z** and **g**⊗**g** denotes the matrix multiplication of **g** with $\mathbf{g}^{\mathbf{T}}$. While this method produced the arrays with the highest resolution, it was the slowest taking several hours. In order to improve its computational efficiency, we first expand equation (4) for $\mathbf{R_{b+1}}$ into the following form.

$$\mathbf{R}_{b+1} = \mathbf{R}_b + \Delta\mathbf{R}_b, \quad \text{where} \quad \Delta\mathbf{R}_b = -\frac{\mathbf{z}\otimes\mathbf{z}}{1+\mu}\mathbf{A}_b + \mathbf{B}_b\mathbf{g}\otimes\mathbf{g} - \frac{\mathbf{z}\otimes\mathbf{z}}{1+\mu}\mathbf{g}\otimes\mathbf{g} \qquad (5)$$

In equation (5) the change in the resolution matrix $\mathbf{\Delta R_b}$ is calculated rather then the entire updated resolution matrix $\mathbf{R_{b+1}}$. The main diagonal elements of $\mathbf{\Delta R_b}$ are calculated one by one, avoiding the use of the temporary matrices $\mathbf{A_{b+1}}$ and $\mathbf{B_{b+1}}$. This reduces the computer time and memory required. The calculations were carried out on a 2.66 GHz Intel i7 Quad-Core system with a Nvidia GTX 285 graphics card. In this test, we use the same damped least squares formulation ($\mathbf{C}=\mathbf{I}$) and damping factor (λ=0.000025) as that used by Wilkinson et al. (2006).

The bulk of the numerical calculations involve matrix-vector multiplications of the form $\mathbf{z}=\mathbf{Bg}$ and $\mathbf{y}=\mathbf{Az}$ (for the first term in $\mathbf{\Delta R_b}$ in equation (5)). A single matrix-matrix multiplication is more efficient than a series of equivalent matrix-vector multiplications. The next step is to calculate the change in the resolution matrix elements for a number of add-on arrays at the same time using the following equations.

$$\mathbf{Z} = \mathbf{BJ} \text{ and } \mathbf{Y} = \mathbf{AZ}, \text{ where } \mathbf{J} = [\mathbf{g}_1\mathbf{g}_2....\mathbf{g}_k] \text{ and } \mathbf{Z} = [\mathbf{z}_1\mathbf{z}_2....\mathbf{z}_k] \qquad (6)$$

The matrix $\mathbf{J}$ is formed from a series of the Jacobian vectors $\mathbf{g_i}$ for k different array configurations. The optimum value for k was found to be 28 for 64-bit Intel CPUs with 16 SSE registers (Leiterman 2005). The CPU used has 4 cores but the Graphics Processor Unit (GPU) has several hundred parallel computational units (Owens et al., 2007). The GPU is limited to simpler numerical operations compared to the CPU but it is well suited for the matrix-matrix calculations. The calculations for 512 configurations can be carried out in parallel using the GPU. This reduces the calculation time by a factor of about 3 (Table 1). The following function F_{CR} is used to the rank the improvement in the model resolution due to an add-on array.

$$F_{CR} = \frac{1}{m}\sum_{j=1}^{j=m}\frac{R_{b+1}(j,j)}{R_b(j,j)} = \frac{1}{m}\sum_{j=1}^{j=m}1+\frac{\Delta R_b(j,j)}{R_b(j,j)} \qquad (7)$$

The change in the resolution $\Delta R_b(j,j)$ can be several orders of magnitude smaller than resolution value $R_b(j,j)$. Thus equation (5) is less sensitive to round-off errors compared to the direct use of equation (4). The calculations for $\mathbf{\Delta R_b}$ are next carried out in single-precision to further reduce the computer time. Table 1 gives the computer time and average relative model resolution ratios achieved by the different versions of the 'Compare R' method. The average relative model resolution is given by $S_r = \frac{1}{m}\sum_{i=1}^{i=m} R_b(i)/R_c(i)$ where $R_b(i)$ and $R_b(i)$ are the base and comprehensive data sets model resolution of the *ith* cell for a model with m cells. The GPU single-precision version is about twice as fast as the double-precision version while differences in the average relative model resolutions are less than 1%. To put the numerical improvements made in perspective, the GPU version takes 33 seconds compared to 3 hours in the original version by Wilkinson et al. (2006) for the 30 electrodes example.

Results

Figure 1a shows a test model with 4 rectangular blocks at different depths in a background medium of 10 Ohm.m below a 2D survey line with 35 electrodes 1 metre apart. Three of the blocks have 100 Ohm.m resistivity. One block has a gradational boundary rising from 20 to 100 Ohm.m to simulate a smooth edge. The first test is with the Wenner array where all the possible measurements are used. The two upper blocks in the resulting inversion model (using a L_1-norm inversion method) after 6 iterations are fairly well resolved while the third deepest block is barely resolved (Figure 1c). In second test all the possible combinations of the '*a*' dipole length and the '*n*' separation factors for a dipole-dipole array (Figure 1b) are used subject to the restriction that the geometric factor does not exceed that that for a dipole-dipole array with '*a*' equals to 1 metre and '*n*' equals to 6 (1056 m). The third deepest block is fairly well resolved but it fails to resolve the deepest block (Figure 1d).

The next test is with the optimised arrays set with 2468 data points using the damped least-squares constraint. The arrays obtained when the average relative resolution ratio reached 0.9 was selected. Figure 2a shows the relative resolution section for this data set. The third deepest block is well resolved with a maximum resistivity of about 39 Ohm.m, and the deepest block is now visible (Figure 1e). The inversion model using a smaller optimised data set (662 data points) also manages to resolve the deepest block (Figure 1f). The final test is with the optimised data sets generated using the smoothness-constrained (L_2-norm) least-squares formulation (Loke at al., 2003). The results (Figures 1g and h) and relative resolution section (Figure 2b) are very similar to those obtained with the damped least-squares method. The deepest block is slightly better resolved where it reaches a maximum value of 19 Ohm.m (Figure 1g). The L_2-norm method minimises the change in the resistivity between adjacent cells, while the damped least-squares method minimises the change in each cell individually. It is possible that the L_2-norm method gives better results for extended structures at depth where the resolution is poor.

Conclusion

Optimised arrays generated by maximising the model resolution have significantly better resolution and deeper depth of investigation compared to conventional arrays for 2D resistivity surveys. The computer time required to generate the optimised arrays is greatly reduced by using parallel numerical algorithms that can make the best use of currently available PC hardware.

References

Auken, E., Pellerin, L., Christensen, N.B. and Sørensen, K. [2006] A survey of current trends in near-surface electrical and electromagnetic methods. *Geophysics*, **71**, G249-G260.

Bingham, D., Nimeck, G., Wood, G. and Mathieson, T. [2006] 3D resistivity in the Athabasca basin with the pole-pole array. *1 day workshop - Geophysical methods and techniques applied to uranium exploration. SEG Annual General Meeting 2006*, New Orleans.

Leiterman, J.C. [2005] 32/64-bit 80x86 assembly language architecture. Wordware Publishing, Inc.

Loke M.H., Acworth I. and Dahlin T. [2003] A comparison of smooth and blocky inversion methods in 2D electrical imaging surveys. *Exploration Geophysics*, **34**, 182-187.

Loke, M. H., Fouzan, F. A. & Nawawi, M. N. M. [2007] Optimisation of electrode arrays used in 2D resistivity imaging surveys. *ASEG 19th Geophysical Conference and Exhibition*, Extended Abstracts.

Owens, J.D., Luebke, D., Govindaraju, N., Harris, M., Krüger, J., Lefohn, A.. and Purcell, T.J. [2007] A Survey of General-Purpose Computation on Graphics Hardware. *Computer Graphics Forum*, **26**, 80-113.

Stummer, P., Maurer, H. and Green, A. [2004] Experimental design: Electrical resistivity data sets that provide optimum subsurface information. *Geophysics*, **69**, 120-129.

Wilkinson, P.B., Meldrum, P.I., Chambers, J.C., Kuras, O. and Ogilvy, R.D. [2006] Improved strategies for the automatic selection of optimized sets of electrical resistivity tomography measurement configurations. *Geophysical Journal International*, **167**, 1119-1126.

Table 1. The times in seconds for 40 iterations (and average relative resolution ratio achieved) for the different versions of the 'Compare R' array optimisation method.

Number of electrodes	Matrix-Vector Double-precision	Matrix-Matrix Double-precision	GPU Matrix Double-precision	GPU Matrix Single-precision
30	202 (0.958)	90 (0.958)	52 (0.958)	33 (0.955)
40	1245 (0.921)	764 (0.921)	335 (0.921)	164 (0.915)
50	6118 (0.886)	4089 (0.886)	1428 (0.886)	620 (0.880)
60	19967 (0.858)	13944 (0.858)	4421 (0.858)	1760 (0.850)

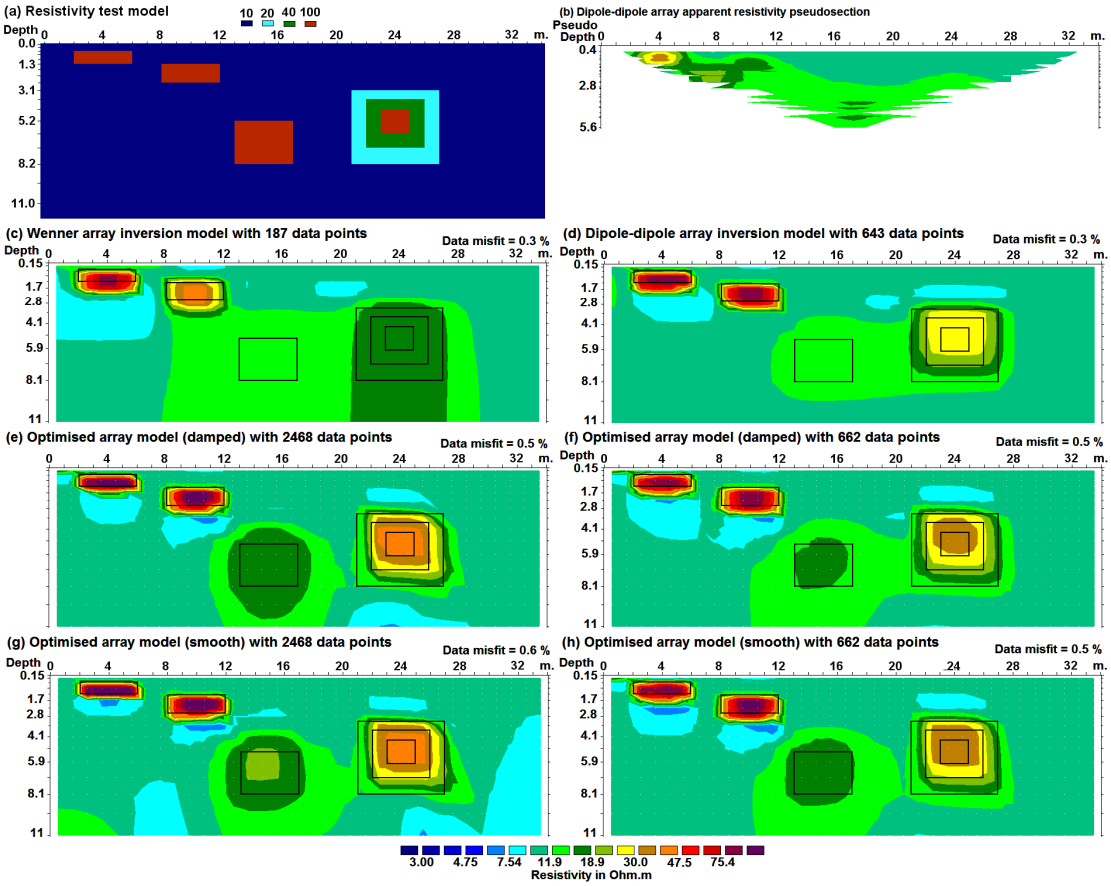

Figure 1. (a) The test model. (b) Dipole-dipole array pseudosection. The inversion model for the (c) Wenner array, (d) dipole-dipole array, (e) large and (f) small optimised array data sets using the damped least-squares constraint, (g) large and (h) small optimised data sets using the smoothness-constrained least-squares equation.

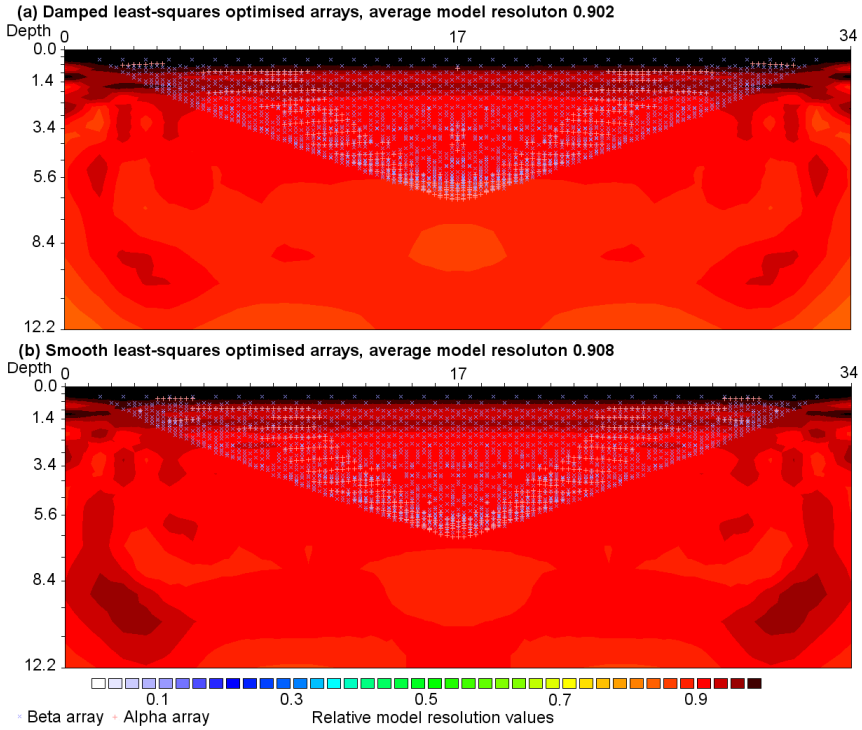

Figure 2. The relative model resolution sections for the optimised data sets using the (a) simple damped and (b) smoothness-constrained least-squares equations.